A DNS/URANS approach for Simulating Rough-Wall Turbulent Flows

F. Alves Portela, N. D. Sandham

Aerodynamics and Flight Mechanics Research Group, Faculty of Engineering and Physical Sciences, University of Southampton, Southampton SO17 1BJ, UK

Abstract

A novel hybrid method combining direct numerical simulation (DNS) and the Reynolds-averaged Navier Stokes (RANS), denoted as a stress-blended method (SBM), has been developed. The SBM is targeted at simulating turbulent flows over arbitrary rough surfaces in which computational savings can be achieved by making the DNS domain as small as possible. Within the SBM framework, a RANS model is enforced above the roughness layer to prevent the momentum build-up which arises in simulations where the computational domain is too small to represent the largest eddies. The SBM is validated for turbulent channel flow, both for smooth wall turbulence and using a parametric forcing approach to mimic roughness effects, with a computational cost that scales linearly with Re_τ. The method is then applied to selected subsets of a scanned grit-blasted surface. For the same subset, the roughness function is found to be within 1% of available DNS. Comparisons of small and large subsets showed differences of over a factor of two in equivalent sand grain roughness, indicating the importance of choosing representative surface samples. Simulations in the fully rough regime are carried out using one to two orders of magnitude fewer points than in a typical DNS. Since no assumptions on the roughness properties or the flow structure (such as outer layer similarity) are made, we expect the SBM to be applicable to non-equilibrium turbulent boundary layer flows.

1. Introduction

The effect of roughness in wall-bounded flows is usually represented by the effective roughness height k_s. The value of k_s corresponds to the roughness height of the sand-grain experiments of Nikuradse [18] which yields the same drag as that of the surface of interest. The drag due to the roughness is usually measured in terms of the roughness function ΔU^+, which is the shift in velocity profiles within the logarithmic region, between the smooth and rough cases [13].

Email addresses: f.alves-portela@soton.ac.uk (F. Alves Portela), n.sandham@soton.ac.uk (N. D. Sandham)

Alternatively, ΔU^+ can also be obtained by considering the difference between the velocities at the centreline of the channel (or at the top of the boundary layer).

Obtaining ΔU^+ for arbitrary surfaces is a cumbersome task both experimentally and numerically. Apart from typical sources of experimental uncertainty, the turn-around for laboratory measurements of ΔU^+ is heavily dependent on wind- or water-tunnel availability and requires manufacturing tiled versions of each surface of interest. On the other hand, numerical approaches to computing ΔU^+ are either limited in terms of Re_τ, in the context of direct numerical simulations (DNS) or the robustness of the turbulence model within the roughness layer, in the context of large eddy simulations (LES) and Reynolds averaged Navier-Stokes models (RANS). Devising novel numerical strategies to tackle the roughness problem is a preferable approach due to growing computational power and the flexibility in manipulating or simplifying the problem setup.

In the context of LES, a rough-wall can either be treated by a wall-model or by fully resolving the turbulence in its vicinity [19]. Naturally, wall-models require some degree of knowledge of the surface properties in order to estimate a value of k_s, e.g. the roughness function should be known *a priori*. In wall-resolved LES the computational costs scale similarly as in a DNS with increasing Re_τ with the added difficulty of choosing models and resolutions capable of handling the inherent anisotropy of the near wall turbulence [1, 5]. Naturally, RANS treatment of near wall turbulence suffers from similar (if not more severe) issues as LES.

Interest in increasing accuracy of flow solutions for industrially relevant Reynolds numbers, not limited to wall turbulence, has pushed for the development of hybrid models in which RANS and LES are used simultaneously in different parts of the flow [see the review by 10]. In wall-bounded turbulence hybrid models usually employ RANS in the vicinity of the wall and "switch" to LES somewhere in the log-layer. As noted by Fröhlich & von Terzi [10] and Hamba [11], a mismatch in the velocity profile develops at the interface between the models, independent of blending function or specific LES/RANS models employed. Hamba [11] bypassed this issue by feeding DNS information to the turbulence models, which is only practical when solving flows for which DNS are available (in which case carrying out turbulence-modelled simulations becomes redundant).

It is thus not surprising that Flack [8] argues DNS should be a necessary component of numerical strategies aimed at determining ΔU^+ for realistic surfaces at industry-relevant friction Reynolds numbers Re_τ. Because a DNS requires resolving all scales of motion, from the viscous length scale δ_ν to the largest eddies which scale with the channel half-height (or boundary layer height) δ, grid sizes and computation time can quickly become too large to efficiently study a broad variety of surfaces.

In-line with the observations above, Chung *et al.* [7] devised a DNS-based approach to computing the roughness function without the typical cost associated with a DNS. Their strategy relies in solving the flow in a channel which is just wide enough to sustain turbulence while being long enough to allow the

flow to fully develop over the roughness elements. The reduced width of the domain allows for cheaper simulations while allowing for ΔU^+ to be computed within the log-layer, since the turbulence becomes unrealistic in the outer layer [14]. The method provides encouraging results [see 17] when using body forces to mimic roughness effects but shows some discrepancies with full-scale DNS when applied to pyramid-like roughness elements.

It should be noted that the approach of Chung *et al.* [7] relies on Townsend's outer-layer similarity hypothesis. Experiments on boundary layers by Krogstad [16] show that the presence of roughness elements can lead to mean velocity profiles which cannot be obtained from their rescaled smooth-wall counterparts. This suggests that the flow characteristics in the vicinity of the roughness elements may depend upon details of those elements and may not be represented by a single parameter, suggesting that values of k_s obtained in channel flows under zero-pressure gradient may not be applicable to more complex flows. It should be noted that, in principle, this is not an issue for the turbulence-model approaches mentioned above (which, as discussed already, suffer from their own complications) but could prevent the method of Chung *et al.* [7] from being applicable to more general problems, since that method relies on Townsend's outer similarity hypothesis.

Drawing inspiration from the methods discussed above, in the present contribution we propose a new method for rough surface simulations in which ΔU^+ can be obtained from simulations using DNS-like resolution but at a fraction of the cost of a typical DNS. The computational savings are obtained by solving the flow in small domains. In order to prevent the flow from laminarising (or becoming incipiently turbulent), we blend the DNS with a turbulence model. Here unsteady RANS models are used to predict the core of the flow. Notice that no assumptions are made with respect to the structure of the surface or the flow properties (such as outer layer similarity).

We begin by outlining the method itself, which we call a stress-blended method (SBM). We then assess the performance of the SBM and the effects of some of the tunable parameters (such as interface shape and location) on smooth-wall simulations. The method is further validated using a parametric forcing approach to mimic roughness effects. Finally we test SBM on a scanned grit-blasted surface for which DNS is available. We conclude by outlining the advantages and limitations of the SBM along with further developments and applications.

2. The Stress-Blended Method

Acknowledging the need to incorporate DNS in calculating the flow over rough surfaces [8], we develop a method which incorporates DNS accuracy at a cheaper (computational) cost that such a DNS would require, by combining the DNS with a turbulence model in a relatively small domain. As will be seen below, the blending (of the DNS with the turbulence model) occurs at the level of the Reynolds stresses and thus we refer to the present approach as the stress-blended method (SBM).

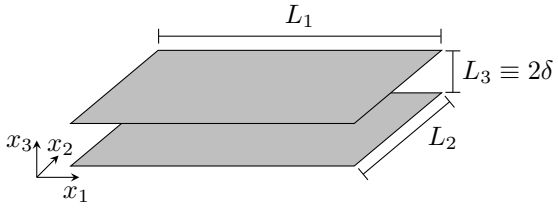

Figure 1: Channel dimensions and coordinate system. δ is the half-channel height.

In order to make the calculation cheaper than a full-scale DNS, we shall follow a similar approach to that of Chung *et al.* [7] by simulating the flow in a relatively small domain. Unlike Chung *et al.* [7], however, the domain is reduced both in the span- and stream-wise directions: i.e. the domain size should be as small as possible to represent the roughness elements of interest and as large as necessary to sustain turbulence in the intermediate near-wall region. Because such small domains will inherently lead to a build-up of momentum in the core of the flow [see 14], we propose incorporating a RANS model into the method, since such models provide realistic descriptions of the mean flow in attached boundary layer flows. The usage of RANS is further motivated in section 3.2 where we show how accurate estimates of ΔU^+ can be obtained with RANS when roughness effects are mimicked through body forces.

In order to incorporate RANS into our DNS, we need to blend the model-free (incompressible) Navier-Stokes equations

$$\frac{\partial u_i}{\partial t} + \frac{\partial u_i u_j}{\partial x_j} = -\frac{\partial p}{\partial x_i} + \nu \frac{\partial^2 u_i}{\partial x_j \partial x_j} + G_i, \tag{1}$$

with the unsteady RANS equation. In the context of turbulent channel flow, this reads

$$\frac{\partial U}{\partial t} + \frac{\partial}{\partial x_3}\left(\nu_t \frac{\partial U}{\partial x_3}\right) = \nu \frac{\partial^2 U}{\partial x_3^2} + G_1, \tag{2}$$

where the spatial coordinates are defined in fig. 1.

In eqs. (1) and (2) $G_i = G_i(t)$ is the driving force which sets the friction Reynolds number ($G_i = 0$ for $i = 2, 3$), $u_i = u_i(x_i, t)$ is the instantaneous fluid velocity, $p = p(x_i, t)$ is the pressure divided by density and ν is the fluid's kinematic viscosity, $U = U(x_3, t)$ is an unsteady mean velocity and ν_t is the turbulent eddy viscosity obtained by means of some RANS model.

2.1. Formulation and governing equations

The first challenge in exchanging information between eq. (1) and eq. (2) is that fields associated with the RANS must involve an averaging procedure. We thus start by defining mean quantities as

$$U_i = \langle u_i \rangle = \iint u_i \mathrm{d}x_1 \mathrm{d}x_2, \tag{3}$$

which are simply averages in the homogeneous spatial directions of the channel (x_1, x_2 as illustrated in fig. 1).

Since eq. (2) is an equation for the mean velocity, the blending with eq. (1) should occur in the average sense. Taking the average of eq. (1) yields

$$\frac{\partial U}{\partial t} + \langle \frac{\partial u_1 u_3}{\partial x_3} \rangle = \nu \frac{\partial^2 U}{\partial x_3 \partial x_3} + G_1, \tag{4}$$

which is in the same form as eq. (2) where the actual turbulent stresses are used instead of modelled. In essence, we shall modify eq. (1) such that, when averaged, it yields either eq. (4) or eq. (2) depending on the region of the flow.

Let us then introduce a blending coefficient $\beta = \beta(x_3)$. We set $\beta = 0$ in regions where the actual turbulent stresses are used and $\beta = 1$ where the RANS model is to be applied; regions where $0 < \beta < 1$ (or where β transitions sharply from 0 to 1) represent the interface. As will be seen below, within the interface β can take any functional form, provided that necessary corrections are applied to the governing equations.

Using this definition of β, a blended equation for U can be obtained by multiplying eq. (2) by β, eq. (4) by $1 - \beta$ and adding the two together. This yields

$$\frac{\partial U}{\partial t} + (1-\beta)\langle \frac{\partial u_1 u_3}{\partial x_3} \rangle - \beta \frac{\partial}{\partial x_3} \left(\nu_t \frac{\partial U}{\partial x_3} \right) = \nu \frac{\partial^2 U}{\partial x_3 \partial x_3} + G_1. \tag{5}$$

Equation (5) is thus a governing equation for the mean velocity which takes in the Reynolds stresses from either the DNS or a RANS model, depending on the value of β. Because eq. (5) is an equation for U, we can now "reverse-engineer' an equation for u_1 which, when averaged, yields eq. (5); the simplest option would be

$$\frac{\partial u_1}{\partial t} + \frac{\partial u_1 u_j}{\partial x_j} - \beta \left[\langle \frac{\partial u_1 u_3}{\partial x_3} \rangle + \frac{\partial}{\partial x_3} \left(\nu_t \frac{\partial U}{\partial x_3} \right) \right] = -\frac{\partial p}{\partial x_1} + \nu \frac{\partial^2 u_1}{\partial x_j \partial x_j} + G_1, \tag{6}$$

with the equations for u_2 and u_3 remaining unchanged.

Equation (6) is thus the governing equation in the SBM. The difference between the eq. (1) (used in a DNS) and eq. (6) is the term $-\beta \left[\langle \frac{\partial u_1 u_3}{\partial x_3} \rangle + \frac{\partial}{\partial x_3} \left(\nu_t \frac{\partial U}{\partial x_3} \right) \right]$, this term effectively sets the mean Reynolds stresses to either the actual turbulent stresses or those obtained by means of a RANS model.

Since RANS models are constructed on the premise that they should provide a realistic picture of the mean flow, we expect that they should cope favourably with the reduction in domain size, which can be problematic in the outer layer; conversely, employing DNS in the roughness layer ensures no details of the flow are lost. Notice that eq. (6) will be solved everywhere within the computational domain and thus all fields remain three dimensional, it is only their averages (in the sense of eq. (3)) that respond to the presence of a model.

2.2. DNS/RANS interface

While eq. (6) reduces to either eq. (1) or eq. (2), depending on whether $\beta = 0$ or $\beta = 1$, it yields neither at the interface. This issue arises due to the fact that $\langle \frac{\partial u_1 u_3}{\partial x_3} \rangle$ is unlikely to be exactly equal to its RANS counterpart, $-\frac{\partial}{\partial x_3}\left(\nu_t \frac{\partial U}{\partial x_3}\right)$. The bulk difference between those two quantities across the interface results in a net driving of the flow, which in turn affects the shear stress at the wall.

This effect can be seen by carrying out a global momentum balance within the channel. Integrating eq. (6) over the whole domain (or equivalently, integrating eq. (5) between the two walls) yields

$$\int_0^{2\delta} \frac{\partial U}{\partial t} \mathrm{d}x_3 - \int_0^{2\delta} \beta \left[\langle \frac{\partial u_1 u_3}{\partial x_3} \rangle + \frac{\partial}{\partial x_3}\left(\nu_t \frac{\partial U}{\partial x_3}\right) \right] \mathrm{d}x_3 = \nu \frac{\partial U}{\partial x_3}|_{x_3=2\delta} - \nu \frac{\partial U}{\partial x_3}|_{x_3=0} + G_1 2\delta. \quad (7)$$

Using the chain rule and noting that $\nu_t = 0$ and $u_1 = 0 = u_3$ at the walls, the second integral in the equation above can be re-written as

$$-\int_0^{2\delta} \frac{\partial \beta}{\partial x_3}\left(\langle u_1 u_3 \rangle + \nu_t \frac{\partial U}{\partial x_3}\right) \mathrm{d}x_3, \quad (8)$$

whose integrand is non-zero only at the interface, where $\frac{\partial \beta}{\partial x_3} \neq 0$.

Defining $x_3^{\beta 1}$ and $x_3^{\beta 2}$ as the interface bounds[1], taking the time average (indicated by $\bar{\cdot}$) of eq. (7) eliminates the transient term and by making use of the channel's symmetry eq. (7) becomes

$$-\int_{x_3^{\beta 1}}^{x_3^{\beta 2}} \frac{\partial \beta}{\partial x_3}\left(\langle \overline{u_1 u_3} \rangle + \overline{\nu_t \frac{\partial U}{\partial x_3}}\right) \mathrm{d}x_3 = -\nu \frac{\partial \overline{U}}{\partial x_3}|_{x_3=0} + G_1 \delta. \quad (9)$$

The driving force G_i is often chosen to be constant, such that it balances out the right hand side of eq. (9), yielding u_τ^2/δ (where u_τ is the friction velocity). The approach here is to make $G_1 = G_1(t)$ and set it to $u_\tau^2 \delta$ minus the contribution due to the SBM, given by eq. (8). Notice that in the case where the interface is sharp ($x_3^{\beta 1} = x_3^{\beta 2}$) eq. (8) gives the exact difference between the DNS and RANS Reynolds stresses at the interface.

The effect of interface was assessed by using both a sharp and smooth interface defined through

$$\beta(x_3) = \begin{cases} 0 & x_3 \leqslant x_3^{\beta 1} \\ \sin^2\left(\frac{x_3 - x_3^{\beta 1}}{x_3^{\beta 2} - x_3^{\beta 1}} \frac{\pi}{2}\right) & x_3^{\beta 1} < x_3 < x_3^{\beta 2} \\ 1 & x_3 \geqslant x_3^{\beta 2} \end{cases} \quad (10)$$

[1] In the case of channel a second interface exists bounded at $2\delta - x_3^{\beta 2}$ and $2\delta - x_3^{\beta 1}$.

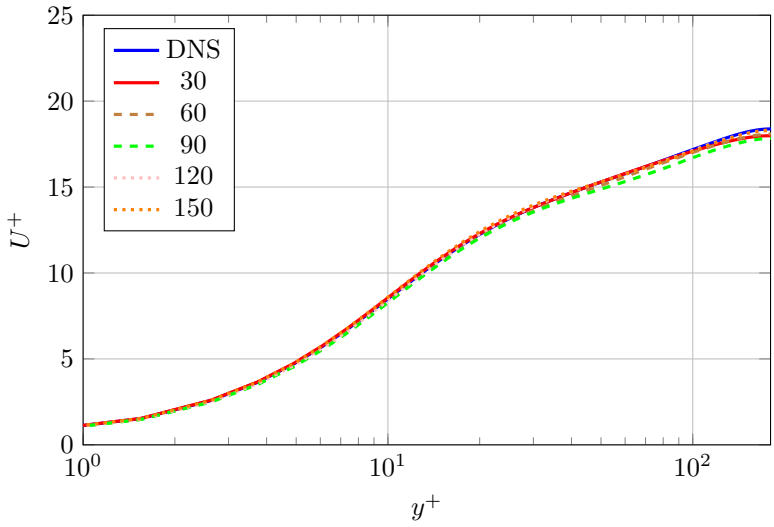

Figure 2: Comparison of mean velocity profiles using SBM with a sharp interface (see legend for interface location) and using DNS at $Re_\tau = 180$.

and by varying the wall distance of the interface (or the mid-point of the interface in the case of eq. (10)). The simulations were carried out with $Re_\tau = 180$ and interface was always located above the buffer region; the SBM simulations used a domain with dimensions $[\pi, \pi/2, 2]\delta$ whereas the DNS simulations used instead $[2\pi, \pi, 2]\delta$. Figures 2 and 3 show, respectively, the mean velocity profiles for sharp and smooth interfaces with the interface location varying from 30 to 150 wall units. As seen in figs. 2 and 3, no significant differences are observed in the mean velocity profiles and thus, for simplicity, a sharp interface is used for the remainder of this paper.

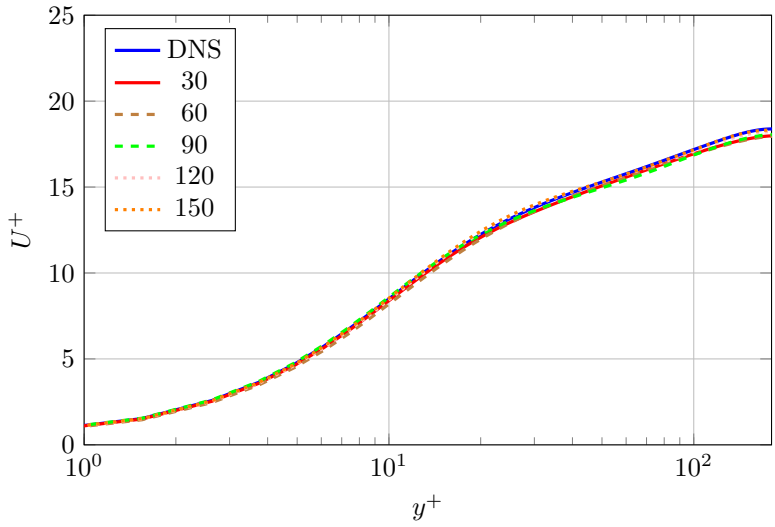

Figure 3: Comparison of mean velocity profiles obtained with SBM with $x_3^{\beta 2} - x_3^{\beta 1} = 10\delta_\nu$ in eq. (10) and using DNS at $Re_\tau = 180$. The legend indicates the location of the interface $\frac{x_3^{\beta 2} + x_3^{\beta 1}}{2}$ for the SBM.

3. Numerical method

All simulations were carried out using second-order accurate finite-differences on a staggered grid for the spatial discretisation and a second-order accurate Adams-Bashforth method for the time integration. The grid is always stretched in the wall-normal direction using a hyperbolic tangent. For the smooth wall and parametric forcing cases the grid spacing varied between δ_ν at the wall and $4\delta_\nu$ at the centreline, whereas for the surface scan cases the resolution was kept constant within the roughness layer and then stretched further away from the wall. For the rough wall cases, the no slip condition is imposed using the immerse boundary method developed by Busse *et al.* [2].

Smooth wall and parametric forcing simulations were carried out in the configurations given in table 1; these were chosen in order to assess the performance of SBM in obtaining accurate mean velocity profiles from relatively small domain sizes. Cases A and C represent typical domains/grids used in full scale DNS while cases B, D and G represent domain sizes approaching the so called minimal flow unit [15]. All simulations were run long enough to overcome the initial transient and statistics were calculated over at least 30 times units (δ/u_τ) with averages taken in the stream- and span-wise directions as well.

In addition to the smooth and parametric forcing simulations, the SBM was also tested by simulating the flow over a grit-blasted surface. The chosen surface has been extensively studied by Busse *et al.* [4] by means of DNS and is thus an ideal test case for assessing the performance of the SBM on realistic flows. Further details on those simulations are given in the relevant section later.

Case	Re_τ	$[L_1, L_2, L_3]/\delta$	$[L_1, L_2, L_3]/\delta_\nu$	$[N_1, N_2, N_3]$
A	180	$[2\pi, \pi, 2]$	$[1130, 565, 360]$	$[128, 128, 128]$
B	180	$[\pi, \pi/2, 2]$	$[565, 283, 360]$	$[64, 64, 128]$
C	360	$[2\pi, \pi, 2]$	$[2261, 1130, 720]$	$[256, 256, 256]$
D	360	$[\pi, \pi/2, 2]$	$[1130, 565, 720]$	$[128, 128, 256]$
E	360	$[\pi/2, \pi/4, 2]$	$[565, 283, 720]$	$[64, 64, 256]$
F	720	$[\pi/2, \pi/4, 2]$	$[1130, 565, 1440]$	$[128, 128, 512]$
G	720	$[\pi/4, \pi/8, 2]$	$[565, 283, 1440]$	$[64, 64, 512]$

Table 1: Domain sizes and resolution used for smooth wall and parametric forcing simulations.

3.1. Parametric forcing

In validating the SBM the effect of roughness was firstly introduced using the parametric forcing approach developed by Busse & Sandham [3]. This is done by adding a source term to the momentum equation of the form

$$- \alpha_i F_i(x_3, h) u_i |u_i|, \tag{11}$$

without summing over repeated indices and where α_i represents the magnitude of the force, F_i is a shape-function which depends on the wall-normal distance (x_3) and the roughness height h. For simplicity, the coefficients α_i were all set to 1 and a box profile was used for F_i.

While parametric forcing could, in principle, be used to model particular rough surfaces, the link between α_i, F_i, h in eq. (11) and the statistical properties of a given surface is not known [3]. Nevertheless, since the flow statistics resemble those of flows over rough surfaces (without the constraint of incorporating a specific surface in the simulation) eq. (11) presents an ideal platform to assess the performance of SBM since the domains can be minimised. Conversely, when considering the flow over a rough surface, reduction in domain size may result in loss of important details of the surface resulting in different roughness functions (as will be seen in section 4.4).

In the present work eq. (11) is useful in assessing the performance of the SBM as it provides a simple framework for varying k^+ and thus obtaining ΔU^+ curves as a function of k^+ for the different configurations listed in table 1. Furthermore, in the context of validating the SBM, the parametric forcing approach removes possible complications associated with choosing representative portions of scanned surfaces.

As will be seen below, RANS simulations were also carried out in support of the SBM approach. Due to the nature of RANS, only the contribution of the mean velocity to eq. (11) (i.e. $-\alpha F(x_3, h)\overline{U}|\overline{U}|$) was used. While Forooghi *et al.* [9] have shown that the neglected contribution is small but not negligible, this issue only persists for RANS simulations, since, in SBM the full (mean and fluctuating) velocity component is available.

3.2. RANS

Two RANS models have been assessed, which are known to provide good results for turbulent channel flow: the algebraic mixing length model (ML)

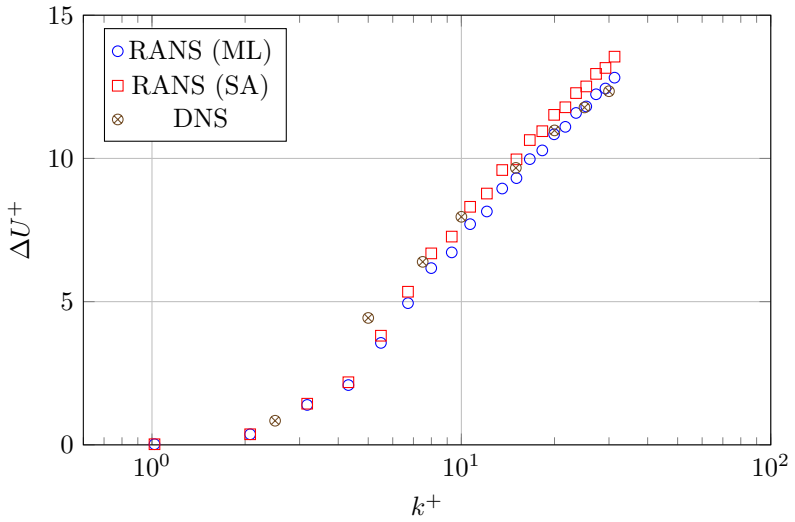

Figure 4: Centreline velocity deficit obtained with full scale DNS and RANS at $Re_\tau = 180$ with parametric forcing.

using the van Driest damping function [*cf.* pp. 302, 366-368 in 19] and the one-equation model by Spalart & Allmaras [20] usually referred to as Spalart-Almaras model (SA). Notice that the SBM is not limited to these particular models and can, in principle, be used with any RANS model.

Independent RANS simulations using the parametric forcing approach described above yielded ΔU^+ vs k^+ curves reasonably close to those obtained by full scale DNS, as seen in fig. 4, which shows the roughness function ΔU^+ as a function of k^+ for multiple RANS simulations. This provides some confidence that RANS is useful for the roughness problem, provided it has a realistic wall friction value. As seen in that figure, both models are practically indistinguishable in the hydrodynamically smooth range of k^+ and are fairly close to the DNS. At higher k^+ the curves corresponding to the RANS simulations display a higher slope than those corresponding to the DNS, this is likely due to the missing contribution from the turbulent fluctuations. Furthermore, both models seem to enter the transitionally rough regime at slightly different values of k^+, with SA appearing to be closer to the DNS for $k^+ \sim 10$ than ML.

Recall that the model results in fig. 4 were obtained with purely RANS simulations. This means that the turbulent component of eq. (11) was not available and thus the forcing used was $-\alpha_i F_i U U$. Nevertheless, the exercise above serves to illustrate that RANS is capable of predicting the shift in mean velocity so long as the correct resistance is imposed within the roughness layer, i.e. without the need to explicitly incorporate that shift in the RANS calculation.

Preliminary simulations using both ML and SA with the SBM showed that the latter coped better with the smallest domain sizes, particularly at higher values of Re_τ. This is likely due to the algebraic nature of the model and the

fact that in ML the eddy viscosity is an explicit function of the mean velocity, whereas SA actually provides an evolution equation for ν_t. For the remainder of this paper all SBM results were obtained with SA.

4. Results

To validate the new approach, we first compare the accuracy of SBM with regards to DNS and RANS in smooth wall turbulence. Simulations were carried out as shown in table 1 with domain sizes substantially smaller than those required for a full scale DNS. These simulations were of both smooth wall turbulence as well as using the parametric forcing approach described above. Finally as simulation of the flow over a grit-blasted surface was carried out, spanning $Re_\tau = 180, 360, 720$ and keeping the domain size constant in terms of wall units.

4.1. Smooth wall

First, the SBM simulations of case A (which corresponds to a full scale DNS configuration) were carried out are compared to the corresponding DNS and RANS (using the same grid). The resulting mean velocity profiles are shown in fig. 5 as well as mean velocity profiles obtained from independent RANS simulations (using the same grid in the wall-normal direction). In fig. 6 the turbulent intensities obtained with SBM and compared to DNS (these are not available in the RANS-only simulations).

Figures 5 and 6 show that the SBM yields almost the same mean velocity and turbulent fluctuations profiles as DNS. Recall that figs. 5 and 6 correspond to the full scale configuration (case A). Nevertheless, this figure illustrates that the introduction of the blending of the RANS with the DNS has little effect on the statistics of the flow and yields better results than independent RANS (admittedly, at the same cost as the DNS in this case). Simulations were also carried out for case B, where the mean velocity profiles from both the DNS and SBM showed no significant differences with respect to case A and therefore are not included here. Figures 5 and 6 show no difference between the SBM simulations using either of the RANS models. For the remainder of this paper the Spalart-Allmaras model is used since it proved to be more robust for small-domain cases, as mentioned already. Finally, it is interesting to note that the SBM does not affect the turbulent properties of the flow, provided that the domain is large enough.

It should be noted that the dimensions of case B are quite close to the minimal channel dimensions proposed by Jiménez & Moin [15]. As such, shrinking the domain size beyond that of case B could lead to laminarisation. For higher Re_τ, where the turbulence sustains, the reduction of domain led to an increase of the velocity profile in the wake region of the DNS. Figure 8 makes this issue very evident. In that figure, the mean velocity profile obtained with the DNS in configuration G barely displays a log-law, contrary to that obtained with the SBM which falls very closely onto the DNS curve extracted from Hu *et al.* [12].

Finally, the turbulent statistics for $Re_\tau = 720$ are shown in fig. 9 for full-scale DNS along with SBM and DNS simulations carried out in smaller domains.

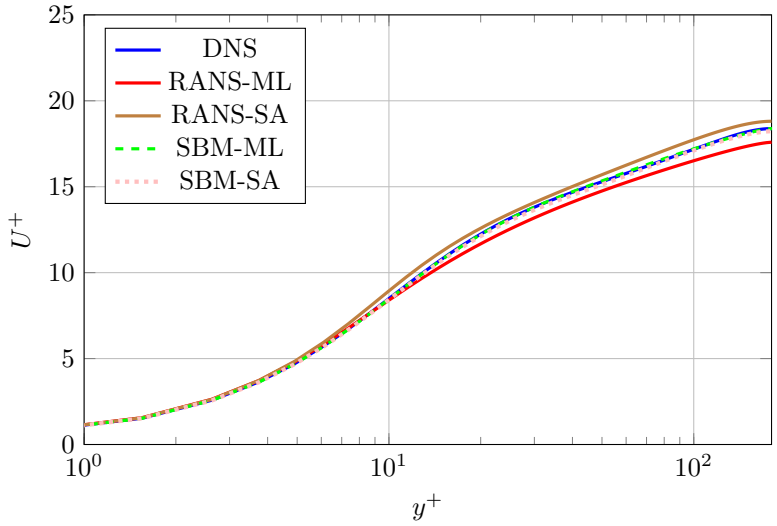

Figure 5: Mean velocity profiles for configuration A (see table 1) at $Re_\tau = 180$.

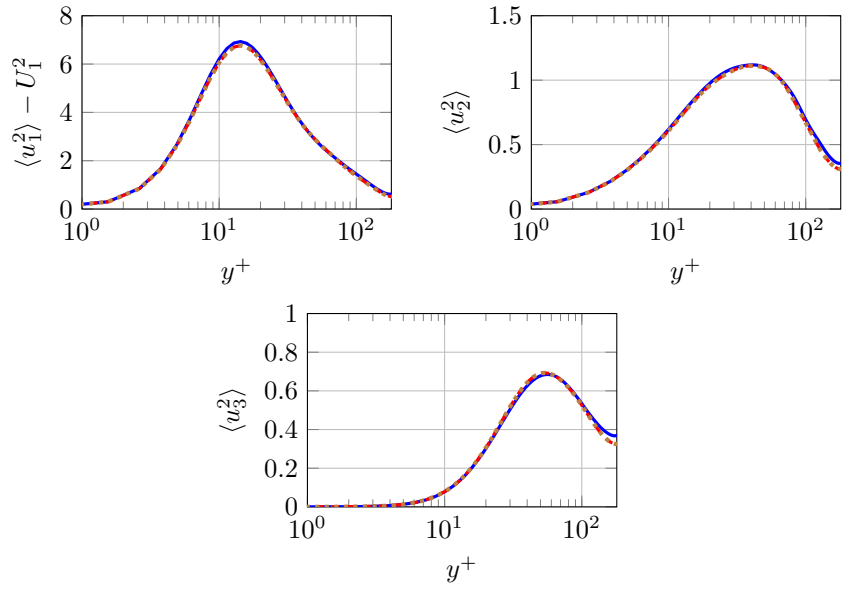

Figure 6: Turbulent intensities for configuration A (see table 1) at $Re_\tau = 180$. See fig. 5 for legend.

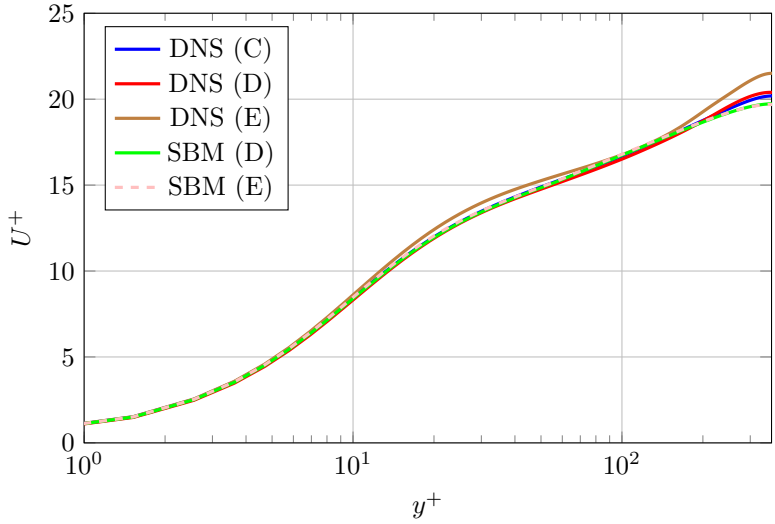

Figure 7: Mean velocity profiles for smooth wall turbulence at $Re_\tau = 360$ (see table 1).

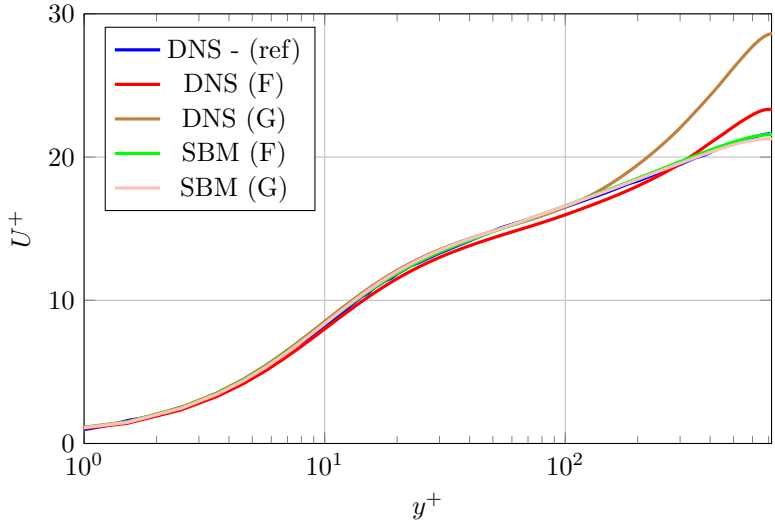

Figure 8: Mean velocity profiles for smooth wall turbulence at $Re_\tau = 720$ (see table 1). The DNS - (ref) profile was extracted from Hu *et al.* [12] and corresponds to a full scale DNS.

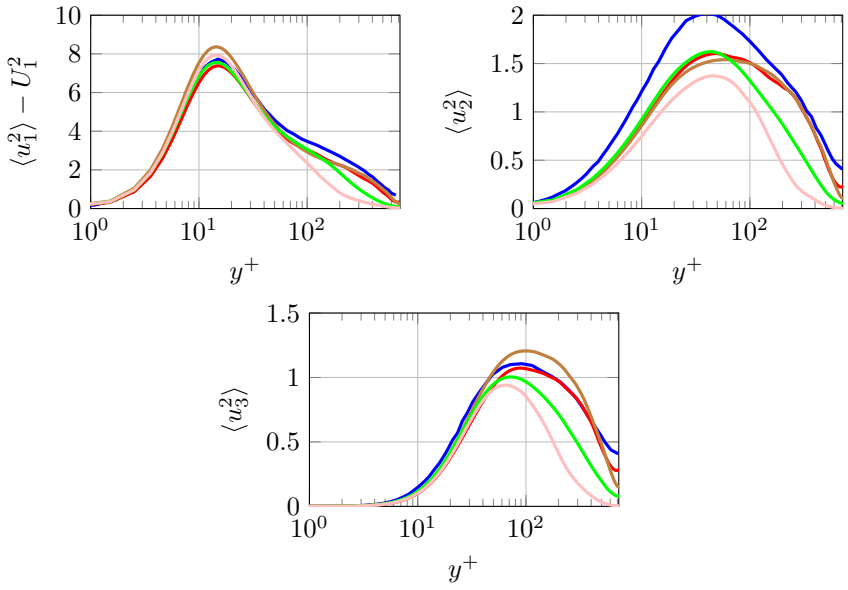

Figure 9: Turbulent statistics for smooth wall at $Re_\tau = 720$. See fig. 8 for legend.

Notice that, unlike for configuration A (recall fig. 6), there is no longer a good agreement with the full-scale profiles obtained with DNS. This is a direct consequence of the fact that the computational domain is insufficient to fully represent all turbulent motions, and, in the case of the SBM, the fact that the chosen turbulence model does not affect these statistics (i.e. it only models the diagonal of the Reynolds' stress tensor).

4.2. Parametric forcing

Further SBM simulations were carried out using the parametric forcing approach section 3.1. The different coefficients were set to $\alpha_i = 1$ and F_i was set to a top hat profile such that $F_i = 1, y^+ < 2k^+$.

For reference, full-scale DNS simulations were carried out for the $Re_\tau = 180$ and $Re_\tau = 360$ cases (i.e. A and C in table 1). Figure 11 shows the variation of ΔU^+ with k^+ obtained with the SBM and compared to the full-scale DNS at $Re_\tau = 360$. An excellent match between SBM and DNS values of ΔU^+ can be observed in that figure. Notice from fig. 11 that, even when the flow domain is shrunk by a factor 4, in the stream- and span-wise directions, the SBM yields near DNS values of ΔU^+. This is also illustrated in fig. 12 where the velocity profiles obtained with the SBM in small domains are very close to those obtained by DNS in large domains. The values of ΔU^+ obtained for cases F and G also showed no significant dependence on the domain size when using the SBM. Figure 11 also shows how SBM and the minimal channel approach of MacDonald *et al.* [17] yield similar values of ΔU^+ when using parametric forcing.

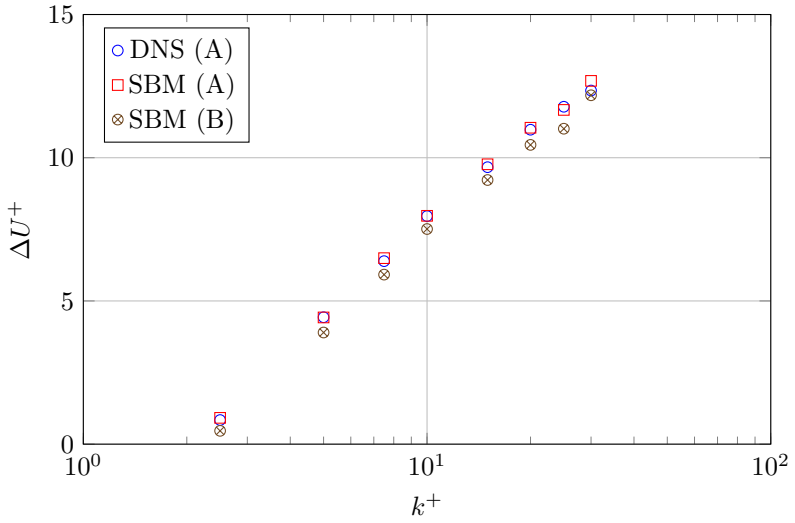

Figure 10: ΔU^+ vs k^+ using parametric forcing for cases A and B with $Re_\tau = 180$.

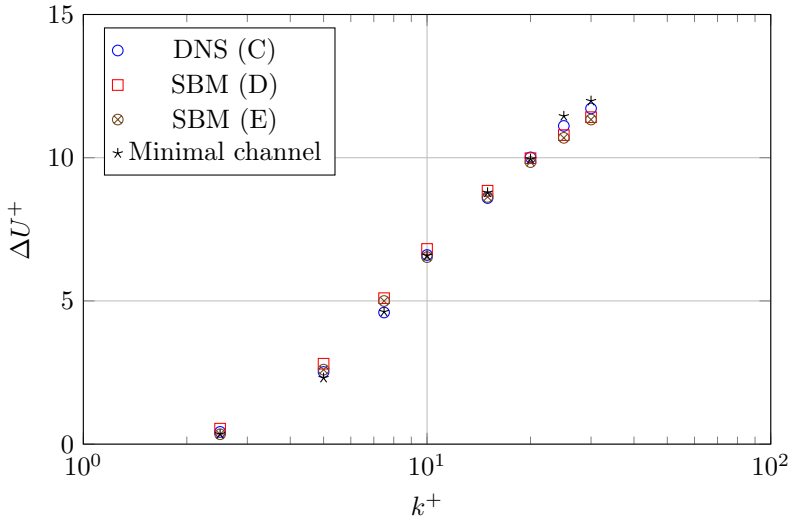

Figure 11: ΔU^+ vs k^+ using parametric forcing for cases C, D and E with $Re_\tau = 360$. Minimal channel results were obtained with the method of MacDonald *et al.* [17] using domain dimensions of 3708 by 117 (in wall units) in the stream- and span-wise directions, respectively.

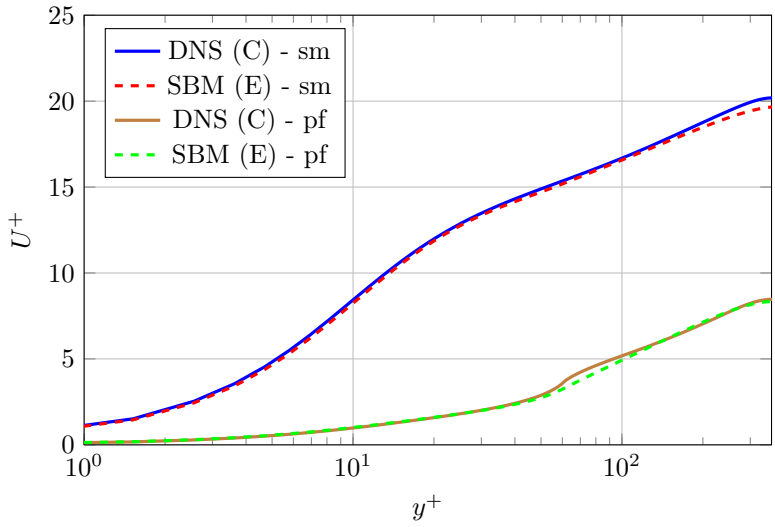

Figure 12: Comparison of mean velocity profiles between cases C and E ($Re_\tau = 360$), using DNS and SBM respectively. The different pairs of curves correspond to smooth wall (sm) and parametric forcing (pf).

4.3. Flow over a grit blasted surface: effect of blockage

Finally, the SBM was employed in solving the flow over a scanned surface. A grit-blasted surface from Thakkar [21] was chosen. The SBM simulations were carried out on a sample smaller (by a factor of 4 in area) than that used in the full-scale DNS of Thakkar [21] as illustrated by a comparison of the solid and dashed lines in fig. 13; Thakkar [21] studied the same small sub-sample, but only at $Re_\tau = 180$. The selection of the sub-sample follows a methodology which scans a given surface with a pre-defined window and finds the sub-sample that best matches the overall properties of the large surface. The same methodology was then repeated for a smaller domain, resulting in the "small sub-sample". Statistical properties of the surfaces are shown in table 2. The surfaces have similar statistical properties, but, as we shall see later, the differences result in different values of the roughness function. As will be seen below, the statistical differences between these samples are not negligible in practice.

Figure 14 compares the mean velocity profiles obtained with the SBM and the DNS results of Thakkar [21] at $Re_\tau = 180$ as well as the profiles obtained by SBM for $Re_\tau = 360$ and $Re_\tau = 720$. For the case where DNS data is available, excellent agreement is observed between the DNS and the SBM.

Table 3 summarises the data shown in fig. 14 in terms of ΔU^+ and flow configurations. Since k^+ is kept constant, one would expect ΔU^+ to remain constant with varying Reynolds number. The small variations in ΔU^+ between the different Re_τ can thus be attributed to the variation in blockage, which was also observed in the blockage study of Thakkar [21]. The results indicate that errors of less than 4% in ΔU^+ are incurred for blockage factors up to $k/\delta = 0.13$.

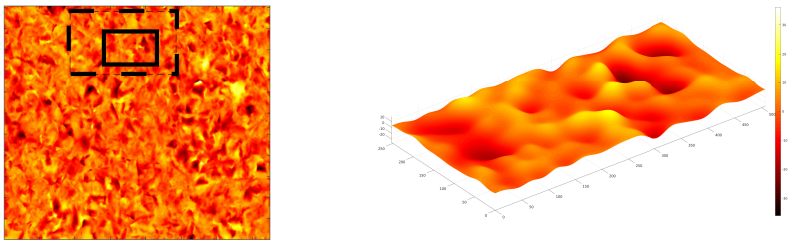

Figure 13: On the left, the scanned surface along with the large sub-sample studied by Thakkar *et al.* [22], highlighted by the dashed line, and the smaller sub-sample studied here, highlighted by the full line. On the right, a perspective view of the small sub-sample (full line on the left).

	Original scan	Large sub-sample	Small sub-sample
L_x/δ	14.1	5.6	2.8
L_y/δ	10.4	2.8	1.4
Sk.	-0.5	-0.5	-0.7
Ku.	4.0	3.8	3.8
$k_{5\times5}/\delta$	0.31	0.17	0.13
k_{max}/δ	0.55	0.26	0.25
k_{rms}/δ	4.3×10^{-2}	3.6×10^{-2}	3.7×10^{-2}
ℓ_x^{cor}/δ	0.26	0.22	0.18
ℓ_y^{cor}/δ	0.25	0.29	0.35
ES_x	0.34	0.23	0.26
ES_y	0.34	0.22	0.23

Table 2: Some properties of the different sub-samples (see fig. 13) of the grit-blasted surface.

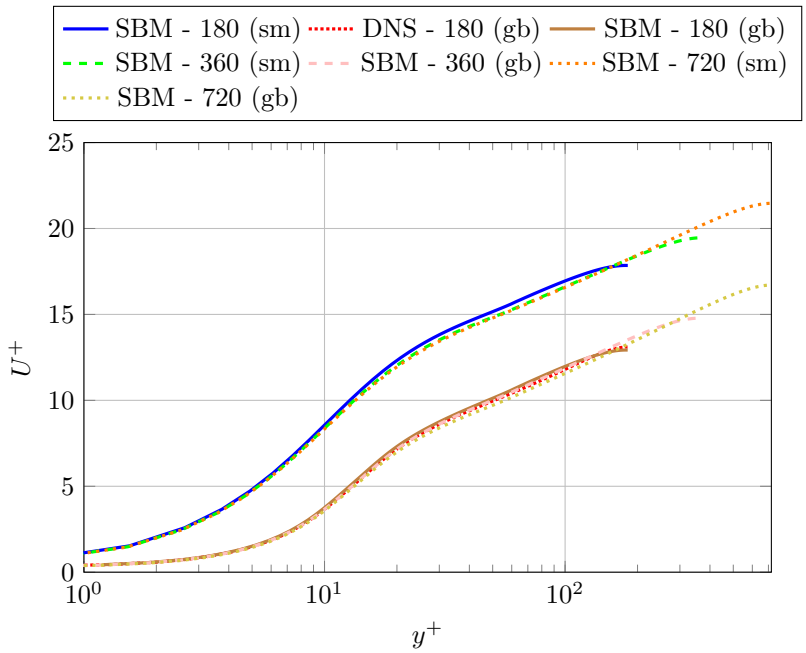

Figure 14: Mean velocity profiles of flow over a grit-blasted surface (gb) and smooth wall (sm).

Re_τ	U_c^+	ΔU^+	L_1/δ	L_2/δ	k^+	k/δ
180	12.93	4.93	2.8	1.4	23	0.13
360	14.78	4.80	1.4	0.7	23	0.06
720	16.60	4.76	0.7	0.35	23	0.03

Table 3: Flow configurations and corresponding ΔU^+ for grit-blasted simulations.

At $Re_\tau = 180$, the centreline velocity deficit ΔU^+ obtained with the SBM was of 4.93, below the value of 5.33 reported by Thakkar [21]. However, it should be noted that reference smooth velocity used in Thakkar [21] was not obtained in such a small domain (but rather from configuration A), if the same reference is used here, the value of ΔU^+ for $Re_\tau = 180$ obtained with the SBM is actually 5.26.

4.4. Flow over a grit blasted surface: grid study

Having determined that for the sample studied here only small blockage effects are observed for $k/\delta < 0.13$, a second study was carried out where the sample dimensions were fixed in terms of half-channel height while Re_τ was increased. This is equivalent to increasing k^+ and allows one to compute the roughness function and therefore the equivalent sandgrain roughness height for this particular sample.

Re_τ	k^+	$\Delta x^+, \Delta y^+$	Δz^+_{min}	Δz^+_{max}	ΔU^+
180	23	3.2	0.7	4	4.9
360	46	6.3	1.4	9.5	7.2
360	46	6.3	0.7	4.7	7.2
360	46	4.2	1.4	9.5	7.4
360	46	4.2	0.7	4.7	7.3
360	46	3.2	0.7	4.7	7.5
720	92	12.7	2.7	19.2	9.5
720	92	8.4	1.3	9.4	9.9
720	92	8.4	0.7	4.7	10.4
720	92	4.2	0.7	4.7	10.3
1440	184	25.3	5.3	38.4	11.2
1440	184	16.9	1.4	9.5	11.9

Table 4: Configurations used for grid study simulations.

For each Re_τ different resolutions were tested (see table 4). The purpose of this was two-fold: firstly, to test the resolution recommendations of Busse *et al.* [2] and secondly, to check the robustness of the SBM approach. The stream- and span-wise resolutions were varied between 3.2 and 12.8, in wall units, and the location of the first grid point was varied between 0.7 and 5.6 (in the most extreme case), also in wall units, with uniform spacing within the roughness layer. Busse *et al.* [2] recommends that the resolution in the stream- and span-wise directions should be the smallest value between $\sim 5\delta_\nu$ and $12/\lambda_{min}$, where λ_{min} is the smallest wavelength used to represent the surface. At sufficiently high Re_τ it becomes possible the violate the latter while still satisfying the former, which is what was done here.

Table 4 also shows the values of ΔU^+ obtained for each case, which are plotted in fig. 15 along with the results of Thakkar *et al.* [22]. It should be noted that the small scatter in the present results did not display any trend dependent on the resolution and can be attributed instead to statistical convergence. When shifted to Nikuradse's data (see right side of fig. 15) it can be seen that the highest Re_τ (equivalently k^+) simulations are already in the fully rough regime. For the highest k^+, the number of grid points used was 64 times smaller than what would be required by a full-scale DNS.

Comparing the present results with those of Thakkar *et al.* [22] in fig. 15 reveals that different values of ΔU^+ are obtained for the two sub-samples. In fig. 16 we show velocity profiles obtained on each sample for similar values of k^+. It is clear that, despite being extracted from the same surface scan, the differences in statistical properties of the two samples shown in table 2 lead to substantially different mean velocity profiles. As such, the equivalent sand-grain roughness obtained in each sub-sample is different; by anchoring the largest values of ΔU^+ to the fully rough asymptote for the sand-grain roughness experiments of Nikuradse [18] (setting the von Kármán constant to 0.4 and the wake parameter to 5.5) we obtain $k_s/k_{5\times5} = 2.1$ and $k_s/k_{5\times5} = 0.87$ for the

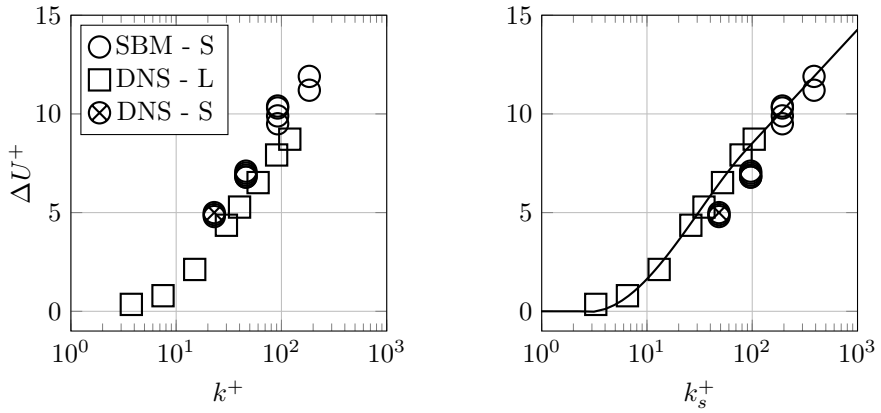

Figure 15: Roughness functions for the small (S) and large (L) sub-samples shown in table 2 from the DNS of Thakkar *et al.* [22], Thakkar [21] and SBM (see table 4). On the left k^+ is equal to $k^+_{5\times5}$, on the right, k^+ is re-scaled to Nikuradse's data (indicated by the full line) through expression (6.5.9) from Cebeci & Bradshaw [6]. For the small sample, computed both with SBM and DNS (SBM - S and DNS - S), $k_s/k_{5\times5} = 2.1$; for the large sample computed with DNS (DNS - L) $k_s/k_{5\times5} = 0.87$.

small and large samples, respectively. Furthermore, the choice of $k_{5\times5}$ as a roughness height measure for the small sample may be inappropriate, as this quantity would be dominated by any prominent features when considering small samples of a given surface [21].

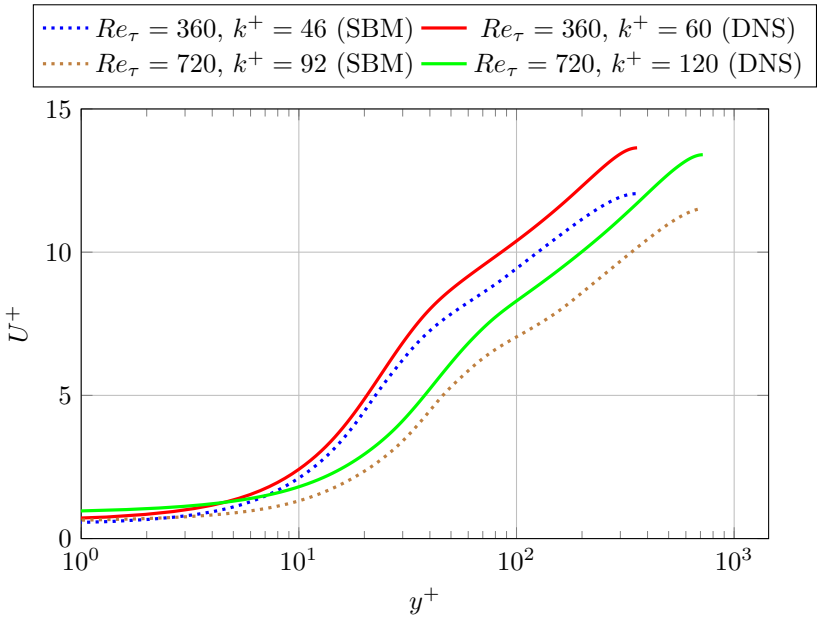

Figure 16: Mean velocity profiles of flow over a grit-blasted surface for increasing Re_τ (and k^+). Only the curves obtained in the finest grids from table 4 are shown. DNS results were obtained on the Thakkar *et al.* [22] on the large sub-sample whereas SBM results were obtained on the small sub-sample (recall fig. 13 and table 2).

5. Conclusion

A novel hybrid method for tackling wall-bounded turbulent flows, called stress-blended method (SBM), has been presented. The method relies on exchanging the Reynolds stresses between the DNS and RANS regions over an interface.

Preliminary tests show that the shape and size of the interface have little effect on the flow, for interface locations within the log-layer. The mismatch between the DNS and RANS stresses over the interface requires special considerations with regards to the overall momentum balance as it results in an artificial driving of the flow. The present approach does not appear to suffer from the same interface issues of other RANS/LES hybrid methods [10].

When the SBM was employed in full-scale simulations the resulting mean velocity profiles are almost the same as those obtained with DNS. As predicted by Jiménez & Moin [15], shrinking of the domain results in laminarisation of the flow near the core of the channel, which manifests itself in the increased wakes obtained by DNS. However, for flows computed through SBM, no such increase in the wake profiles was observed and, in fact, the mean velocity profiles were found to be close to the full-scale DNS profiles.

The performance of SBM in the presence of roughness was further validated by means of the parametric forcing approach of Busse & Sandham [3]. The SBM was able to accurately predict the added resistance in domains up to 8 times smaller (in the stream- and span-wise directions) than a full-scale DNS would require. In such cases, the computational costs is effectively $1/64$ of the DNS. These results are in-line with the minimal channel results of MacDonald *et al.* [17] who are able to achieve similar savings for parametric forcing simulations. Similar savings (in terms of domain size) were obtained when the SBM was applied to a blockage study of the flow over a grit-blasted surface. Furthermore, when varying the grid resolution up to 5 wall-units (in terms of the first grid point) values of ΔU^+ were found to fall within 1% of the DNS results (for the same sample) obtained by Thakkar [21].

It was observed that by simulating a much smaller sample a different value of the equivalent sand-grain roughness was obtained. The difference in k_s can be explained on the basis of different topological properties of the surfaces and the choice of reference roughness height. The success of SBM in predicting k_s for an arbitrary surface thus appears to rely on how closely the simulated surface represents that for which one seeks to know k_s (notice that this wouldn't be an issue for regular roughness). For example, isolated features (such as the prominent valley identified in fig. 13) are likely to exert larger influence in flows over smaller domains than in their larger counterparts. This potential shortcoming highlights the need for further understanding the relationship between a surface's topological properties and k_s (or ΔU^+). This is currently ongoing work.

6. Acknowledgements

The authors acknowledge the support of EPSRC through the grant number EP/P009638/1 and the computational resources allocated in ARCHER HPC through the UKTC funded by the EPSRC grant number EP/R029326/1.

[1] Baggett, JS, Jimenez, J & Kravchenko, AG 1997 Resolution requirements in large-eddy simulations of shear flows. *Annual research briefs* pp. 51–66.

[2] Busse, A., Lützner, M. & Sandham, N. D. 2015 Direct numerical simulation of turbulent flow over a rough surface based on a surface scan. *Computers & Fluids* **116**, 129 – 147.

[3] Busse, A. & Sandham, N. D. 2012 Parametric forcing approach to rough-wall turbulent channel flow. *Journal of Fluid Mechanics* **712**, 169–202.

[4] Busse, A., Thakkar, M. & Sandham, N. D. 2017 Reynolds-number dependence of the near-wall flow over irregular rough surfaces. *Journal of Fluid Mechanics* **810**, 196–224.

[5] Cabot, W. & Moin, P. 2000 Approximate wall boundary conditions in the large-eddy simulation of high reynolds number flow. *Flow, Turbulence and Combustion* **63** (1), 269–291.

[6] Cebeci, Tuncer & Bradshaw, Peter 1977 *Momentum transfer in boundary layers*.

[7] Chung, D., Chan, L., MacDonald, M., Hutchins, N. & Ooi, A. 2015 A fast direct numerical simulation method for characterising hydraulic roughness. *Journal of Fluid Mechanics* **773**, 418–431.

[8] Flack, K. A. 2018 Moving beyond Moody. *Journal of Fluid Mechanics* **842**, 1–4.

[9] Forooghi, P., Frohnapfel, B., Magagnato, F. & Busse, A. 2018 A modified Parametric Forcing Approach for modelling of roughness. *International Journal of Heat and Fluid Flow* **71** (March), 200–209.

[10] Fröhlich, J. & von Terzi, D. 2008 Hybrid les/rans methods for the simulation of turbulent flows. *Progress in Aerospace Sciences* **44** (5), 349 – 377.

[11] Hamba, F. 2003 A hybrid rans/les simulation of turbulent channel flow. *Theoretical and Computational Fluid Dynamics* **16** (5), 387–403.

[12] Hu, Z., Morfey, C. L. & Sandham, N. D. 2006 Wall pressure and shear stress spectra from direct simulations of channel flow. *AIAA Journal* **44** (7), 1541–1549.

[13] Jiménez, J. 2004 Turbulent flows over rough walls. *Annual Review of Fluid Mechanics* **36** (1), 173–196.

[14] Jiménez, J., Flores, O. & García–Villalba, M. 2001 The large-scale organization of autonomous turbulent wall regions. *Tech. Rep.*. Center for Turbulence Research.

[15] Jiménez, J. & Moin, P. 1991 The minimal flow unit in near-wall turbulence. *Journal of Fluid Mechanics* **225**, 213–240.

[16] Krogstad, P-Å. 1992 Comparison between rough-and smooth-wall turbulent boundary layers. *Journal of Fluid Mechanics* **245**, 599–617.

[17] MacDonald, M., Chung, D., Hutchins, N., Chan, L., Ooi, A. & García-Mayoral, R. 2017 The minimal-span channel for rough-wall turbulent flows. *Journal of Fluid Mechanics* **816**, 5–42.

[18] Nikuradse, J. 1950 Laws of flow in rough pipes. *NACA* .

[19] Pope, S. B. 2000 *Turbulent Flows*. Cambridge University Press.

[20] Spalart, P. R. & Allmaras, S. R. 1992 A one-equation turbulence model for aerodynamic flows. In *30th aerospace sciences meeting and exhibit*, p. 439.

[21] Thakkar, M. 2017 Investigation of turbulent flow over irregular rough surfaces using direct numerical simulations. PhD thesis, University of Southampton.

[22] Thakkar, M., Busse, A. & Sandham, N. D. 2018 Direct numerical simulation of turbulent channel flow over a surrogate for nikuradse-type roughness. *Journal of Fluid Mechanics* **837**, R1.